UKAEA FUS 393

UKAEA Fusion
(UKAEA/Euratom Fusion Association)

A novel plasma-wall instability and the distribution of halo currents in tokamaks

A Caloutsis and C G Gimblett

February 1998

UKAEA
Fusion

Culham Science Centre, Abingdon
Oxfordshire, OX14 3DB
United Kingdom
Telephone +44 1235 463311
Facsimile +44 1235 463647

A Novel Plasma-Wall Instability and the Distribution of Halo Currents in Tokamaks

A. Caloutsis and C.G. Gimblett
UKAEA, Fusion, Culham Science Centre, Abingdon
Oxon, OX14 3DB, U.K.
(UKAEA/Euratom Fusion Association)

Abstract
It is recognized that tokamak plasma disruptions and vertical displacement events, with the attendant appearance of 'halo currents', are a threat to future experiments such as ITER. Halo currents, flowing between the plasma and the wall, can develop large spatially localized components. Here, we ascribe this to a new instability that can occur in a composite circuit of a magnetized plasma and a solid conductor. The presence of the conductor divides the current perturbation into topologically distinct stable and unstable composite plasma-wall circuits. The plasma paths of such circuits are subject to hydromagnetic motions, which alter circuit geometry and conductivity while self-consistently preserving toroidal and poloidal periodicity. We develop a simple prototype model which illustrates the geometrical aspect of the mechanism. The heterogeneity of the true plasma-wall system is shown to introduce considerable complexity. Our basic concept may underlie a wider class of instabilities and waves.

I Introduction

Tokamak plasmas can be unstable to an axisymmetric vertical motion which, in the absence of any restraining effect, would proceed on a fast Alfvénic time scale [1]. Surrounding the plasma with a passive conducting structure (field windings, vacuum vessel *etc.*) increases the time scale of the instability to a much longer one related to the resistive penetration time of the 'wall'. Due to its relatively slow growth there is the practical possibility of controlling this positional instability using suitable externally applied correcting fields. Occasionally however, perhaps due to failure of the position control system or a stability limit being exceeded, vertical control is lost and an instability known as a Vertical Displacement Event or VDE can develop. The VDE can lead to the plasma coming into contact with the wall, the formation of so-called 'halo' currents, and ultimate plasma disruption. Halo currents are currents flowing in circuits between the outer plasma and the wall, and have been observed in some experiments to develop large toroidally asymmetric components.

The VDE/disruption sequence has various deleterious practical consequences. Thermal loads are placed on divertor target plates and other parts of the external structure,

leading to erosion and vaporization. Voltages generated by the plasma motion can lead to localized arcing, and the considerable Lorentz forces that develop (as in the JET experiment [2]) can lead to structural failure. As well as being important for present day experiments, elementary scaling arguments based on force balance indicate that these effects will be more serious for next-generation tokamaks such as ITER [3]. For an early review of these topics see [4], for recent experimental results from COMPASS-D and Alcator C-MOD see [5], [6], and for a world-wide summary for use in the ITER design see [7].

Halo currents often develop large asymmetric components which can exacerbate the above mentioned effects. Present modelling of halo currents assumes that the asymmetry comes from the core plasma itself becoming unstable to an MHD kink mode, but the observed relative amplitude of shift and tilt displacements appears inconsistent with this [8]. Here, we propose a mechanism underlying the formation of halo asymmetry in terms of a hybrid instability, caused by an interaction between the outer layers of the plasma and the wall, where the main plasma column remains stable. In our picture, the basic eigenmode requirements of toroidal and poloidal periodicity and electromagnetic and kinematic self-consistency are met in a special way by the three-dimensional juxtaposition of magnetized plasma and solid conductor.

In Section II we isolate the deformation of the plasma-wall contact, or 'footpoint motion', one of the novel aspects of the instability deriving directly from the compound nature of the plasma-wall circuit, and in Section III construct, as an example, a simplified model of a poloidal halo that exhibits the expected behaviour. To gain insight into the process, a linear perturbation analysis is carried out, and the resulting analytic stability boundaries are compared with numerical output, finding qualitative agreement.

In Section IV we suggest how the proposed instability would operate in the practically relevant case of a helical halo. We complete our outline of the full mechanism, not captured by our example model, with a qualitative argument about the origin of the plasma drift velocities, responsible for 'footpoint motion' and changes in the conductivity of the halo plasma. Issues discussed in this section are the current distribution in the wall, the reaction of the core plasma to the halo current, and the periodicity of the perturbed current path. General conclusions are presented in Section V.

II The mechanism of 'footpoint motion'

Halo currents flow helically within a doubly connected annulus enclosing the disrupting toroidal core plasma. The annulus is composed of a plasma sector and a wall sector meeting on inboard and outboard contact loci that initially form toroidal circles, see fig. 1a. The plasma sector is an outer layer of the core plasma with magnetic surfaces intersecting the wall, permitting current to flow into the wall sector, around the core, and reenter the halo plasma on the opposite side. We assume that both sectors are sufficiently thin for their contacts to be considered lines. Driving primary voltages exist due to the changing magnetic fluxes in the enclosed disrupting core, and the usual toroidal drive.

For simplicity, we first consider the artificial case where current and magnetic field lines are entirely poloidal, and the equilibrium magnetic field is sufficiently large that

current perturbations in the halo do not significantly change it. We may then regard the halo current distribution as a multiplicity of closed filamentary poloidal current circuits, stacked along the toroidal direction, each comprising a plasma path and a wall path connected in series.

An initial deformation of the inboard and outboard contact loci, hereafter 'footpoints', will then clearly change both the resistance and inductance of an individual filament, by changing the lengths of both the wall and plasma paths, characterized by different resistivities, see fig. 1b. This will change the current in the filament, while the existing inductance will retard the change. We now assume that the footpoint positions are determined by local force balance in the halo plasma, and that changing current can change, via force balance, the average radial position of the plasma path (due to underlying plasma drifts). The plasma-wall contact will then move according to the wall shape. Critically, if force balance is such that the change in current reinforces the initial deformation then instability becomes possible. A toroidal wavelength arises because the filaments are linked via mutual inductances, and thus partially 'mirror' the current changes in their neighbours. The result is an inductive ripple, with filaments 'dumping' current on their neighbours, changing their 'L/R' time via footpoint motion, and leading to further dumping.

To predict the outcome, we must calculate such changes in resistance and inductance in detail. However, because of the heterogeneity of the plasma-wall system there is no simple coordinate system in which to solve globally. The partly ad hoc model we solve below serves to illustrate the generic principle of the inductive ripple via footpoint motion.

III A prototype model

We consider a straight vessel, with periodicity length L. The halo equilibrium fields are entirely poloidal, invariant along the 'toroidal' direction $\hat{z}$. We postpone a physical discussion of how force-balance links changes in filament current to changes in filament size, as required to complete the feedback, but introduce instead a parameter of 'positional gain' in an ad hoc manner. A specific mechanism will be suggested in Section IV on the helical halo, as it requires separate physics.

A Ohm's law

The current in each composite infinitesimal filament, introduced above, obeys the circuit equation

$$\Omega_z \, i_z = -\frac{\partial}{\partial t}\Phi_z + V \, . \tag{1}$$

We adopt the convention that the subscript z refers to toroidal position (not direction), so that $\Omega_z \equiv \Omega(z,t)$ is the *poloidal* resistance per unit toroidal length at location z, $i_z \equiv i(z,t)$ the *poloidal* current per unit toroidal length, $\Phi_z \equiv \Phi(z,t)$ the *toroidal* flux linked by the filament, due to halo currents everywhere, and V the constant poloidal driving voltage, common to all filaments. Figure 1a shows a schematic drawing of a toroidal cross-section.

We assume that the inboard and outboard plasma-wall contacts of a filament are at mirror-symmetric positions described by a minor radius $y_z \equiv y(z,t)$, equal to the distance

between a contact and the centre of the plasma core. We write

$$\Omega_z = \Omega + \rho \Delta y_z \quad \text{where} \quad \rho = \eta/\delta \,. \tag{2}$$

Non-subscripted parameters, as above, will refer to equilibrium values. Ω is the initial effective resistance of the mixed circuit per unit toroidal length and ρ its rate of change with plasma radius, as the lengths of the wall and plasma paths are modified. η is an effective resistivity and δ an effective width, introduced only to make the dimensions of the 'filament resistance' Ω explicit. The precise value of ρ will strongly depend on the difference between plasma and wall conductivities and on the angle of incidence of the magnetic field on the wall surface. Also, inhomogeneities of material, wall thickness or structure may exist between inboard and outboard contacts, influencing these effective values.

B Inductive coupling

To model inductive couplings we adopt expressions available for coaxial circular rings; see for instance [10]. Calculation of mutual inductances in non-trivial geometries requires numerical treatment.

Given a current loop of radius $a_z \equiv a(z,t)$ –note index convention– situated in the poloidal plane at z, the flux linked by a coaxial test loop of radius $a_{z'}$ situated at a distance $x = z' - z$ –see also figure 1b– is given approximately by $\Phi_{zz'} \equiv \Phi(z, z', t)$, where

$$\Phi_{zz'} = \mu_0 I_z \sqrt{a_z a_{z'}}\, F_{zz'} \,, \tag{3}$$

with

$$F_{zz'} = \frac{1}{2} \ln \left[16 \frac{(a_z + a_{z'})^2 + (x + \delta_w)^2}{\kappa^2} \right] - 2 \,, \tag{4}$$

and

$$\kappa^2 = (a_z - a_{z'})^2 + (x + \delta_w)^2 \,, \tag{5}$$

where I_z is the current in the loop. $\Phi_{zz'}$ diverges logarithmically with decreasing κ, as the test loop experiences an increasingly singular current distribution. We have expressed the toroidal inter-loop distance as $x + \delta_w$, adding a small but non-zero wall thickness δ_w. This persists as the characteristic length of the radial width of a current loop in the limit of $x \to 0$, preventing an artificial singularity in the value of filament self-inductance (in principle, the thickness of the halo plasma could play a similar role, but we assume that the wall dominates the effect). Expression (4) is only valid near a filament. The corresponding expression at large distances is listed in Appendix A.

We may suppose that the coaxial filaments are generally non-circular and expand in a lop-sided way as contacts move on the wall surface. To account for non-uniformity, we introduce an effective induction radius a_z for a composite coil at z, related to variations of the plasma radius y_z, defined previously, by

$$a_z = a + l \Delta y_z \,, \tag{6}$$

where a is the initial effective radius, l is the 'inductive gain', analogous to ρ of eqn. (2), and dependent on geometry, for instance on the relative sizes of the immovable wall path

and the movable plasma path. It is possible that the values of a and l are influenced by special structures existing between inboard and outboard contacts.

The original induction equation, (1), gives rise to an integral equation, holding at all z,

$$(\Omega + \frac{\rho}{l}\Delta a_z) i_z = -(\mu_0 F)\frac{\partial}{\partial t}\int_{-L/2}^{L/2} i_{z'}\sqrt{a_z a_{z'}}\, M_{zz'}\, d(z'-z) + V\,, \tag{7}$$

where $M_{zz'} = F_{zz'}/F$ is a coupling coefficient normalized to the equilibrium value of $F_{zz} \equiv F$, according to equations (4, A2).

C Force balance

Closure of the system (7) requires a relation between filament size and current, which is in principle provided by considerations of force-balance.

For our example model, however, we choose the simplest possible closure scheme, namely a linear relation between $\Delta a_z \equiv a_z - a$ and Δi_z, by introducing a constant 'positional gain parameter' s_0, of unspecified value. This is defined at equilibrium by the relation

$$\frac{\Delta i_z}{i} = -s_0 \frac{\Delta a_z}{a}\,. \tag{8}$$

s_0 is thus assumed to contain all information about the (saturated) amplitude of the induced plasma drift, which effects force-balance, the amount of pressure sustainable in the halo due to transport, and the consequences of these for footpoint motion given the geometry of the wall-field intersection. We will return to consider the physical basis for a positional gain in our discussion of the instability in the real halo, in Section IV, where it will become apparent that this is especially complicated.

D Numerical solution

In numerically solving the system (7, 8) we used spatial grids with 20-50 points and time steps of the order of a few percent τ_0, defined below. Denser space-time grids yield similar results. Figures 3–6 show the numerical evolution of the instability for different values of the initial inductive aspect ratio ($\mathcal{A} \equiv L/a$) and the postulated positional gain (s_0). The instability grows out of small random perturbations of the filament currents and a single wavelength becomes dominant. The most obvious interpretation is that there is a characteristic distance, of the order of the halo minor radius, over which the inductive coupling between a pair of filaments decays, and thus the wavenumber is determined by the number of times this distance fits inside the toroidal periodicity length. This number should be large for large aspect ratio and vice versa. However, the following linear stability analysis shows that very strong determinants of stability are also the positional gain s_0, and the ratio τ_0/τ_1 of global and local timescales, defined below. There is a tendency for the asymmetry to become increasingly peaked with time, as the dominant current channel drains current from its neighbours on all length scales.

E Linear stability analysis

We normalize the system (7, 8) using for current, effective coil radius, and position the non-dimensional quantities α_z, g_z, $\bar{z}$ defined by

$$\alpha_z = a_z/a\,, \quad g_z = i_z/i\,, \quad \text{and} \quad \bar{z} = z/L\,, \tag{9}$$

and define

$$\tau_0 = \frac{\mu_0 F L}{\Omega/a}\,, \quad \tau_1 = \frac{\mu_0 F L}{\rho/l}\,, \tag{10}$$

which are global and local 'L/R' characteristic timescales; see also equations (2, 6).

We consider small perturbations of current and effective radius, and linearize around a toroidally symmetric equilibrium to find at each toroidal position z

$$\frac{\partial}{\partial t}(\Delta g_z)\int_{-1/2}^{1/2}(M_{zz'}+2M'_{zz'})\,d\bar{x} - \int_{-1/2}^{1/2}((2s_0-1)M_{zz'}-2M'_{zz'})\frac{\partial}{\partial t}\Delta g_{z'}\,d\bar{x} = \frac{2(s_0-\tau_0/\tau_1)}{\tau_0}\Delta g_z\,, \tag{11}$$

where $\bar{x} = \bar{z}' - \bar{z}$. We have eliminated α using relation (8) in the form $\Delta g_z = -s_0\,\Delta\alpha_z$.

The quantity $M'_{zz'} = \partial M_{zz'}/\partial\alpha$ is the rate of change of the coupling coefficient $M_{zz'}$ with coil effective radius α, at equilibrium. It is not necessary to distinguish between α_z and $\alpha_{z'}$ because of the reciprocity of mutual inductances and the toroidally symmetric initial conditions. Introducing a dependence

$$\Delta g_{z'} \propto \cos[2\pi n(\bar{z}+\bar{x})]\,\exp(\gamma_n t) \tag{12}$$

for $n = 0, 1, 2, \ldots$, it is straightforward to show that eqn. (11) yields a dispersion relation

$$\gamma_n[I_1 + 2I_2 + (1-2s_0)I_3 + 2I_4] = \frac{2(s_0-\tau_0/\tau_1)}{\tau_0}\,, \tag{13}$$

where

$$I_1 = \int_{-1/2}^{1/2} M_{zz'}\,d\bar{x} \sim \frac{\mathcal{A}_t/\mathcal{A}}{|\ln(\delta_w/a)|} \tag{14}$$

$$I_2 = \int_{-1/2}^{1/2} M'_{zz'}\,d\bar{x} \sim \frac{\mathcal{A}_t/\mathcal{A}}{2|\ln(\delta_w/a)|} \tag{15}$$

$$I_3 = \int_{-1/2}^{1/2} M_{zz'}\cos(2\pi n\bar{x})\,d\bar{x} \sim \frac{\mathcal{A}_t/\mathcal{A}}{|\ln(\delta_w/a)|}\,\widehat{\mathrm{Si}}(n\pi\mathcal{A}_t/\mathcal{A}) \tag{16}$$

$$I_4 = \int_{-1/2}^{1/2} M'_{zz'}\cos(2\pi n\bar{x})\,d\bar{x} \sim \frac{\mathcal{A}_t/\mathcal{A}}{2|\ln(\delta_w/a)|}\,\widehat{\sin}(n\pi\mathcal{A}_t/\mathcal{A})\,. \tag{17}$$

The analytic approximations on the right of the above list are further discussed in Appendix B. $\mathcal{A} = L/a$ is the 'inductive aspect ratio' of the halo, the ratio of the toroidal periodicity length to the initial effective poloidal filament radius. The approximations above are valid for $\mathcal{A} > \mathcal{A}_t \sim 2.6$, where $\mathcal{A}_t$ is a characteristic aspect ratio defining the

transition from an inductively 'strongly coupled' to a 'weakly coupled' halo. The value 2.6 is specific to a coaxial-ring geometry, representing the ratio of the length over which $M_{zz'}$ decays, to the filament radius. We thus specialize to the case of a weakly coupled halo. Further validity conditions are

$$\delta_w \ll a\,, \quad \text{and} \quad L/(2\pi n) \gg \delta_w\,, \tag{18}$$

specifying a thin wall, and excluding wavelengths so short that they compete with the filament radial thickness. Finally, we have defined the functions

$$\widehat{\sin}(x) \equiv \frac{\sin x}{x} \qquad \text{and} \qquad \widehat{\mathrm{Si}}(x) \equiv \frac{1}{x}\int_0^x \frac{\sin t}{t}\,dt\,, \tag{19}$$

the sine and sine-integral normalized by their argument. Both functions tend to unity as their argument tends to zero, and tend to zero as their argument tends to infinity ($\widehat{\mathrm{Si}}(x)$ tends to $\pi/2x$).

The growth rate, given by eqn. (13), can then be evaluated using expressions (14) to (17), together with (10) and (B1), to find approximately

$$\gamma_n \sim \tau_h^{-1}\,\frac{(s_0 - P)}{(R(u) - s_0)}\,\frac{1}{\widehat{\mathrm{Si}}(u)}\,, \tag{20}$$

where

$$\tau_h = \frac{\mu_0\, a}{(\Omega/\mathcal{A}_t a)} \tag{21}$$

roughly corresponds to the 'L/R' timescale of a solenoid of radius a and length $\mathcal{A}_t\, a$ which, as mentioned above, is the characteristic decay length of inductive coupling along the poloidal halo.

The remaining factors of expression (20) govern stability, with $u = n\pi\mathcal{A}_t/\mathcal{A}$ and

$$R(u) = R(\mathcal{A}, n) = \frac{\widehat{\mathrm{Si}}(u) + \widehat{\sin}(u) + 2}{2\widehat{\mathrm{Si}}(u)}\,, \tag{22}$$

where $R(0) = 2$, while

$$P = \frac{\tau_0}{\tau_1} = \frac{a/l}{\Omega/\rho} \tag{23}$$

is a 'resistance parameter' of the halo. Equation (20) shows $s_0 = P$ is a cut-off while $s_0 = R(\mathcal{A}, n)$ are resonances. Referring back to relations (2, 6) it is easy to see that Ω/ρ and a/l, appearing in the above expression for P, can be thought of as effective resistive and inductive sizes of the halo. If the coils of the halo were homogeneous rings, then $P = 1$. However, the differing coil resistances of the wall and plasma paths, and details of geometry such as the strike angle —see fig. 1a, can not only make $P \neq 1$, but even negative or divergent.

Figure 2 shows the analytic stability boundaries of the first few modes in the $(\mathcal{A}, s_0)$ plane. According to eqn. (20) a mode n is unstable if s_0 lies within the interval $[P, R(\mathcal{A}, n)]$, and stable otherwise. All modes are stable if $s_0 = P$, whereas $s_0 = R$ generates a singularity in the growth rate, discussed below. Numerical results verify these boundaries,

qualitatively, and quantitatively usually to within 30%. The waviness of the stability boundaries is expected, caused by the behaviour of the integrals I_3, I_4 in equations (16, 17): for a given aspect ratio there is a fixed coupling distance over which mutual inductances decay; as n increases, the difference between the coupling distance and the closest integral number of wavelengths oscillates. With increasing aspect ratio the coupling distance progressively becomes much shorter than the wavelengths of an increasing number of harmonics, which become locally indistinguishable. Thus, all $R(\mathcal{A}, n)$ tend to $R(\mathcal{A}, 0) = 2$ as $\mathcal{A}$ tends to infinity. Also, universal stability would be achieved by either lowering s_0 below $R(\mathcal{A}, 0) = 2$ while raising P above s_0, or by having $s_0 = P$.

Figures 3–6 show the initial evolution of the numerical model for different parameter settings, with reference to their position on the analytic stability diagram of figure 2. The results verify the analysis in a qualitative way, showing that as the system is taken across a boundary the corresponding harmonic becomes gradually dominant until it suddenly disappears, while the next harmonic takes over until the next boundary is reached, and so on. The asymmetry becomes increasingly peaked with amplitude because of the increasing inductive dominance of the current channel at the peak of the asymmetry over its immediate neighbours.

The singularities in the growth rate are, of course, unphysical. They arise in this model when the rate of expansion of a filament with changing current changes its inductance at a rate that would be just sufficient to sustain the very same change in current, if coil resistance remained constant. In this limit the system is neutrally stable with respect to current changes, but there is no extra voltage available to drive the current change should the resistance be changing as well. Since resistance does change with filament size, near this limit a divergent rate of expansion becomes necessary to provide the extra voltage. A finite growth rate at such resonances could be restored by amending the model to include drift velocities, recognizing that the adjustment of position through 's_0' implies an unphysical, instantaneous plasma displacement in response to current perturbations.

F Discussion

The example calculated above makes the point that, at least in principle, there is opportunity for instability in a hybrid plasma-wall circuit stemming simply from the reshaping of the wall path by perturbed force-balance in the plasma. However, the issue of the physical origin of contact-motion (s_0), which is a consequence of plasma drifts, cannot be discussed within the above poloidal model, and is taken up in the section on the helical halo below.

It is important to note that the size of the inductive and resistive 'gains' of the plasma-wall circuits can be strongly influenced by the geometry of the intersection of magnetic field and conductor; for instance, a very shallow angle of incidence of the magnetic field on the wall, see fig. 1a, could be made to yield arbitrary, even divergent, values.

We emphasize that the instability does not exist simply because of the mutual back emfs between the circuits –these serve to organize the mode spatially– but because of the permanent gain in the conductivity of a circuit due to its change in shape and size, as in the above model, or due to its accumulation of conducting material, as we shall argue below.

Our use of simple formulae to model inductive couplings, rather than employ Faraday's law, is dictated by the heterogeneity of the system: there is no simple coordinate system, with eigenfunctions, to describe both plasma and wall circuits. This heterogeneity becomes even more critical in the case of a realistic helical halo, below. For example, tracking footpoint motion in the helical case would require knowledge of the pitch of the magnetic field, the pressure in the halo (zero pressure if the halo is force-free), the effect of field perturbations, and the three-dimensional wall shape.

IV The case of the helical halo

We discuss, in qualitative terms, the topology and inductive couplings of helical plasma-wall current circuits, the associated drifts induced in the surrounding plasma, and their capacity to produce instability via both footpoint-motion and the perturbation of halo plasma conductivity. We propose that these separate elements can in practice interact in a self-consistent way, leading to a growing or propagating plasma-wall eigenmode.

A Rationalization via the wall sector

In the poloidal model the plasma-wall current path was automatically closed, but in the helical case the 'rationality' of the composite path (*i.e.* self-closure after toroidal and poloidal revolutions) is less obvious. Since the halo plasma is cooled by wall contact, we may assume it is force-free. If we further assume a sufficiently large equilibrium magnetic field, then both equilibrium and small perturbation currents will tend to flow along it. (A related point concerns the distinction between current across the magnetic field due to 'magnetization' and that due to drift. The latter may enter the wall, as it involves the physical displacement of particles, but the former may not, being an apparent current due to the superposition of localized gyro orbits in the presence of a pressure gradient. When a particle enters the wall a complete gyro orbit is destroyed, and thus no magnetization current is transported across the plasma-wall interface. If we are prepared to ignore the drift component, we can therefore state that the 'halo current' only consists of the force-free component of the plasma current, even in the presence of a significant halo pressure gradient.)

Therefore, in a tokamak the toroidal angle ζ traversed by the force-free current path between inboard and outboard wall contacts will be approximately specified by the pitch of the magnetic lines in the halo plasma sector

$$q_h = B_z/(AB_\theta) \tag{24}$$

(the safety factor), and may be written as

$$\zeta = 2\pi(1-\lambda)q_h\,, \tag{25}$$

where λ is the poloidal angular fraction occupied by the wall sector and A the aspect ratio.

Turning to the wall sector, we see that, given ζ, the toroidal wavenumber and amplitude of a mode inside the halo plasma specify boundary conditions on both inboard

and outboard sides of the wall annulus. Knowledge of the time derivative of the normal magnetic field would then completely specify the streamfunction of the perturbed current inside the wall sector.

A compound plasma-wall surface will therefore act in a way similar to a rational magnetic surface, allowing current perturbations parallel to the field to exist, for any mode number, and for any q_h of the magnetic surface involved. This happens at the price of splitting the mode current into topologically distinct loops. In general, only a fraction of the perturbation current will flow across the wall sector, while the remaining fraction will recross the plasma-wall boundary on the same side.

This is shown in the stationary solution of Figure 7a. The 'helical' channels, connecting across the wall, link the torus both poloidally and toroidally, while the 'surface' channels, connecting on the same side, do neither. This is a fundamental distinction, as only the helical channels can provoke the inductive ripple mechanism of our prototype model, purely on topological grounds. Figure 7b shows a cartoon illustrating the distinction, which carries over to the helical case. The helical channels are inductively linked in the sense required by our inductive-ripple model, where an increase in the current of one channel tends to induce a decrease in the next one. However, as may be verified by inspection of figure 7b, the inductive linkage between surface channels acts in the opposite sense, so that a current increase in one tends to induce a current increase in the next. Surface channels would not, by themselves, grow via the mechanism of the prototype model.

This prompts us to define a mode 'quality factor' Q_n as the ratio of helical to total (helical plus surface) current fluxes. The closer Q_n is to unity, the less energy has to be expended driving the stable surface channels. We may easily calculate a Q_n for the special case of a saturated mode ($\partial_t = 0$) and a flat, annular wall sector with circular plasma-wall boundaries, as shown in figure 7a. By first locating the X-points of the current flow, we find (see also Appendix C) that

$$Q_n = \frac{2(A_w)^{n/2}}{1+(A_w)^n} \left|\cos(n\zeta/2)\right| , \tag{26}$$

with

$$A_w = R_{out}/R_{in} , \tag{27}$$

where R_{in} and R_{out} are the inboard and outboard major radii of the plasma-wall intersection. Expression (26) shows that the value of Q_n is sensitive to the value of ζ. For example, if $\zeta \sim 2\pi$, current is almost entirely poloidal and $n = 1$ gives the largest Q_n (*i.e* most favourable for instability). If $\zeta \sim \pi$, the $n = 1$ mode has no contributing helical component and $n = 2$ is favoured. In general, as either the aspect ratio tightens (*i.e.* A_w increases) or n increases, then Q_n decreases as the current flow completes the circuit along the shortest path.

Expression (26) applies to a simplified case, and does not acknowledge either the existence of eddy currents due to magnetic perturbations normal to the wall, or the deformation of plasma-wall boundaries. If the normal field were known, an eddy current distribution, entirely contained within the annulus boundaries, could be simply superposed on the potential distribution, since the latter already satisfies boundary conditions.

This would, in general, reconnect the total current flow and thus change Q_n. However, (for reasons of energy conservation), growth is not driven by back emfs, but, in our picture, by a subset of plasma-wall circuits becoming better-conducting current paths. The current perturbation caused by the perturbed conductivity alone is, of course, a potential distribution, and, for mode growth, we should expect that the associated back emfs preserve a similar topology, as was trivially the case in the poloidal prototype. We may also argue in reverse that if the mode saturated and were found to be in a stable, low-Q_n, configuration, it would be difficult to see how it could have *continuously* evolved towards it. Thus, the stationary expression given may still retain some correlation with halo instability. The perturbation of the boundaries (footpoint-motion) is not addressed here, but below we shall argue for an important halo 'fueling' process that does not depend upon it.

B The effective q

A global 'effective' q may be defined for the composite helical channels. We introduce a 'wall' q by writing

$$q_w = J_z^w/(AJ_\theta^w)\,, \tag{28}$$

evaluated using only the 'helical' component of the current in the wall, as defined in the previous section. We then find

$$q_{eff} = \lambda q_w + (1-\lambda)q_h = \frac{m}{n}\,, \tag{29}$$

where m and n are the number of poloidal and toroidal crossings of a complete helical circuit. The 'toroidal mode number' is the number of poloidal crossings, n.

We may note here that the most unstable plasma-wall modes may tend to be those with wall current flowing mainly in the poloidal direction, since the quality factor is then likely to be large. Then, from eqn. (29), with q_w small and $0 < \lambda < 1$, q_h will generally be larger than q_{eff}. Thus, as the equilibrium safety factor q_h falls, such modes will encounter rationality before the halo magnetic field itself does. Given that the wall always allows partial (helical) rationalization, we may expect a soft onset of instability as q_h approaches q_{eff} from above.

The effective q is a conserved property of the plasma-wall eigenmode, analogous to the constant wavevector of a helically symmetric plasma mode. We may then regard the requirement $\Delta q_{eff} = 0$ as a first step in the construction of a dispersion relation for the asymmetric plasma-wall mode. Of course, to gain any useful information out of it, we would need to be able to evaluate the variation of the right side of (29) in terms of a growth rate, and the appropriate equations of motion as applied to the plasma-wall system. Given the geometrically complicated way by which plasma flow is generated, discussed below, this probably necessitates numerical modeling. Nevertheless, we may take a first small step in the quantification of $\Delta q_{eff} = 0$, in order to illustrate the issues behind eigenmode self-consistency.

Because of the unfavourable inductive coupling of the surface channels of Section A, we will consider an idealized test-case where the plasma motion associated with a growing mode occurs with the spatial distribution required to exactly preserve the 'helical' identity

of an initial helical perturbation without spilling-over into a surface channel (i.e. $Q_n = 1 = const.$). Under the further assumptions of a force-free plasma and a nearly saturated drift motion on the time-scale of the instability, so that a simple Ohm's law in the field direction may be used in the plasma, we find that in the halo plasma

$$\frac{i_z^p}{i_\theta A} = q_h \,, \tag{30}$$

where q_h is given by eqn. (24). Since all of the poloidal plasma current is assumed to cross the wall sector, eliminating i_θ using $q_w \equiv i_z^w / i_\theta A$ (the continuity of i_θ automatically accounts for voltage redistribution between wall and plasma sectors), we find

$$q_w = q_h \frac{i_z^w}{i_z^p} \,. \tag{31}$$

Ohm's law (without plasma drift) requires

$$i_z^p = (\delta_p/\eta_p) E_z^p \,, \quad \text{and} \quad i_z^w = (\delta_w/\eta_w) E_z^w \,, \tag{32}$$

where $\eta_{p,w}$ are the plasma and wall resistivities. Relation (31) then gives

$$q_w = \hat{\eta} \frac{E_z^w}{E_z^p} q_h \,, \tag{33}$$

which specifies the pitch of the helical current path in the wall, with

$$\hat{\eta} \equiv \frac{\eta_p \delta_w}{\eta_w \delta_p} \,. \tag{34}$$

Substituting relation (33) into (29), we write the q_{eff} of the combined current path as

$$q_{eff} = q_h[(1-\lambda) + \lambda \hat{\eta} (E_z^w / E_z^p)] \,. \tag{35}$$

Since $q_{eff} = m/n$ remains constant, variation of the electric fields during mode evolution must be compensated by variations in either q_h and λ, or $\hat{\eta}$. The first two are functions of the contact point positions, which corresponds to contact motion as in the prototype model. If we emphasize this limit,the 'dispersion relation' secures mode integrity by way of the geometric deformation of the wall and plasma paths, and the growth rate must adjust to this process. The other possibility involves the adjustment of $\hat{\eta}$. If we emphasize this limit, mode integrity is secured via transport. Both processes are the product of plasma drifts, as discussed next.

C Plasma drift and halo 'fueling'

To complete our qualitative argument we now consider the central, kinematic aspect of the instability and the generation of plasma flows according to the MHD ideal term $\mathbf{v} = \mathbf{E} \times \mathbf{B}/B^2$. The key observation, which also distinguishes the plasma-wall instability, is that the symmetric, but generally non-rational, core magnetic field interacts with

electric potentials induced by an adjacent asymmetric but globally rational current density perturbation, which itself achieves rationalization only because of the intrusion of a different medium, here an isotropic ohmic conductor.

The irrational magnetic field inside the core winds through successive regions of positive and negative amplitude of the induced electric field. The induced voltage parallel to the magnetic field is therefore electrostatically cancelled inside the core, since no net current can be driven in that direction, and reappears in the cross-field direction as an electrostatic potential. The total electric field is then entirely across magnetic field lines and causes plasma drifts which deform the core. In particular, radially drifting plasma crosses the plasma-core boundary, leaving the ideally-behaving core and becoming part of the ohmically-behaving halo circuit.

Such core drifts (and drifts inside the halo itself), displace the local plasma-wall contact areas and change their size, as postulated in our prototype model, by moving plasma into or out of successive layers of equilibrium magnetic lines intersecting the wall. The drifts also 'fuel' the cold halo by ejecting hot plasma from the core, locally increasing halo conductivity. They are thus able to provide two distinct kinds of gain for the global conductance of the local plasma-wall circuit, both of which can, in principle, lead to instability. These two aspects were also implied in the requirement for the preservation of q_{eff} of eqn. (35). It is perhaps relevant that results from DIII-D [11] show that during the distinct phases of the thermal quench and the current quench, the degree of halo asymmetry varies from relatively large to relatively small. This is consistent with a scenario where the fueling mechanism attenuates as the core cools, but the geometric aspect of the instability persists.

The above argument establishes the basic reason for the existence of the required flows and their likely effects. Their quantitative impact on the feedback mechanism can be heavily modulated by the specific geometry of the intersection between wall and magnetic field (which becomes itself perturbed), and by the transport laws regulating the evolution of halo plasma conductivity in contact with the wall. These issues are beyond the scope of the present discussion. In terms of the basic self-consistency of our mechanism, the remaining issue is whether it is plausible that the flows can occur with the correct toroidal phase to fuel or deform the corresponding plasma-wall circuit in a positive way.

Dispersion relations commonly specify complex frequencies, when mode propagation and growth must coexist. Within the context of electromagnetism, a combination of real and imaginary parts of the frequency phase-shifts the electric field induced by an evolving current perturbation by $\pi/2$ to $3\pi/2$ —the remaining phase interval being, of course, excluded for reasons of energy conservation. (This is easy to see by evaluating $\nabla \times \nabla \times \mathbf{E} = -\mu_0 \partial_t \mathbf{J}$ for plane-wave eigenmodes.) Although mixing growth and propagation always affords some phase flexibility, phase relations in our case will be also specified by the vector product $\mathbf{E} \times \mathbf{B}$ and the characteristic asymmetry of the mixed-medium circuits. In the absence of an exact calculation it is difficult to give a definite answer. Nevertheless, we may specialize to pure growth, and try to envisage a scenario where the plasma-wall mode self-consistently 'fuels' itself, by inducing the injection of hot core plasma into the halo at the toroidal location of increasing halo current.

Since current perturbations in the force-free halo are approximately parallel to the magnetic field, the electric fields induced in the adjacent layers of the core will cause

Origin of electric field components	*$E \times B$ plasma flows and role in mechanism*
$E1$:Primary induced E-field in the vicinity of the plasma sector.	Associated flows of secondary importance due to near alignment with the B-field. Drives $E3$-5.
$E2$:Primary induced E-field in the vicinity of the wall sector.	Not aligned with nearby B-field. Associated flows as for $E3,4$. Drives $E3$-5.
$E3$: Electrostatic field to maintain continuity of current through plasma-wall interface.	Changes in the induced E-fields are redistributed anisotropically across and along the footpoint locus. The changing direction of the E-field in the halo plasma produces flow and footpoint motion.
$E4$: Electrostatic field resolving the global discrepancy between the core magnetic q and the rational structure of $E1$-3.	Flow is in the wall direction, indirectly driven by $E1$-3. Radial expansion of plasma causes footpoint motion. Expelled hot plasma changes halo conductivity.
$E5$: Surface charges confining current into solid conductor.	Assumed negligible.

Table 1: Summary of origin and effects of perturbation electric fields in the plasma-wall system.

relatively small drifts, which we neglect. This is in contrast to the wall perturbation current which flows in a completely different direction (q_w), so that in the nearby core the induced electric field will have a large component across the core magnetic field, which has constant pitch. This remains true after cancellation of the external halo potentials along core field lines. Following a magnetic field line of the core near the force-free halo shows that charge must accumulate to cancel the approximately constant induced potential. However, in the poloidal sector of the core neighbouring the wall, the pitch of the mode changes drastically, the field line enters a region of opposite induced potential, and thus the gradient of the charge density reverses. This shows that the maxima of the charge density will appear in the vicinity of the wall, and we may expect that the maxima of the resulting electrostatic field across magnetic lines, and of the associated radial drifts, will be similarly localized. This supports what may be perhaps established simply 'by symmetry', namely that plasma drift will mainly occur towards or away from the wall current path, which is where the clash between q_{core} and q_w is poloidally localized. Note that in a vertical disruption these drifts would appear as a characteristic 'tilt' of the plasma column, towards or away from the wall, without the sideways 'shift' of a core kink mode.

The plasma and wall sectors constitute resistors connected in-series. As the plasma conductance increases via fueling, voltages induced around the circuit will be electrostatically redistributed to keep current divergence-free. Consequently, and despite the fact that back-emfs oppose current growth, current and total electric field will always be in the same direction inside and in the vicinity of the wall sector, as required by Ohm's law $E = \eta_w J$. The sense of this electric field (after the in-series plasma-wall redistributions), together with the discrepancy between q_h in the core and q_w in the wall, suggest that inside the section of the core nearest the wall $\mathbf{E} \times \mathbf{B}$ flows are generated that eject plasma, in phase with the growing halo current.

Table 1 summarizes the various electric fields and plasma flows present in the mechanism.

V Conclusions and discussion

The observed toroidal asymmetry of the halo current during a VDE may be attributed to the growth of a special plasma-wall eigenmode which has no direct counterpart in the plasma itself. However, some comparisons with tearing modes can be made, and these may clarify the nature of our argument.

Tearing modes are able to develop magnetic islands, with rational current channels flowing within them, only on special equilibrium magnetic surfaces of rational q. By contrast, in the plasma-wall case, the presence of the conducting wall ensures the rationalization of perturbation current channels on magnetic surfaces with arbitrary q, and irrespective of the formation of an island. The price for this is the splitting of the current into discrete 'helical' and 'surface' channels, with very different topologies. The inductive linkage between the helical channels makes them susceptible to instability, whereas the surface component is stabilizing.

The plasma core, surrounded by the halo annulus, does not have a resonant magnetic surface and reacts 'ideally', generating perturbation flows, much like the plasma regions outside the separatrix of an island in the case of tearing modes. Plasma subsequently crosses the halo-core boundary, fueling the halo circuits, in analogy to plasma crossing into the separatrix of a growing island through magnetic reconnection at X-points.

In the case of tearing modes, magnetic perturbations determine the growth of the necessary rational island, and simultaneously regulate the 'fueling' of a growing island through X-point reconnection due to non-ideal layer physics. The balance between these processes is central to the mechanism, and is usually reduced to the solving of Newcomb's equation in the ideal regions, and the matching to a suitable resonant layer response, all in terms of the magnetic field.

In contrast, the halo rational channels may always exist beyond the first, arbitrary-q magnetic surface intersecting the wall, which is thus externally imposed as a 'separatrix'. Hence, the exact relationship between the the plasma flow amplitude and the field perturbation amplitude generated at the halo-core boundary is not critical for the existence of a plasma-wall mode. Two novel issues arise instead. The displacement of the plasma-wall contact via both field perturbation and plasma flow, leads to geometric changes in the inductance, mutual inductance, and global resistance of the mixed plasma-wall current channels. Also, the sharp density and temperature gradient between the core and the halo leads directly to local changes in halo conductivity, as a consequence of boundary-crossing flows.

In basic terms, the instability operates by changing the 'L/R' timescales of localized plasma-wall current channels, in such a way that a channel becomes more conducting as it gains more current. The inductive transfer of current from less conducting to more conducting channels becomes then self-reinforcing and imposes a global wavelength. We note in passing that even if halo asymmetry were driven by a kink, elements of this mechanism would be likely to become involved.

Because of the three-dimensional interaction of the three distinct parts (the plasma sector, the wall sector, and the core), it is not possible to write down, in a simple way, the equations describing the system, to be solved within a single system of coordinates. At the same time, this asymmetry is central to the existence of the instability. Numerical modelling will thus be required in order to establish the ultimate coherence of our qualitative picture.

Acknowledgements

We are grateful to G.G. Castle for discussions on experimental data from COMPASS-D and START, and to A. W. Morris for useful comments.

This work was funded jointly by the Commission of the European Communities (Contract No. 5004-CT96-5008 (DG 12-MRGS)), the UK Department of Trade and Industry, and Euratom.

References

[1] J.A. Wesson, Nucl. Fusion **18**, 87 (1978).

[2] P. Noll, L. Sonnerup, C. Froger, M. Huguet, and J. Last, Fusion Technology **15**, Part 2A, 259 (1989).

[3] S. Ortolani, P. Barabaschi, N. Fujisawa, M. Rosenbluth, and J. Wesley, "Disruption and VDE Characterization for ITER" in *22nd European Physical Society Conference on Controlled Fusion and Plasma Physics, Bournemouth* (The European Physical Society, Petit-Lancy, 1995), Vol. 19C, Part IV, p. 9.

[4] O. Gruber, K. Lackner, G. Pautasso, U. Seidel, and B. Streibl, Plasma Phys. Control. Fusion **35**, B191 (1993).

[5] G.G. Castle, A.W. Morris, D. Gates, and M. Valovič, "Halo Currents and VDEs in COMPASS-D" in *23rd European Physical Society Conference on Controlled Fusion and Plasma Physics, Kiev* (The European Physical Society, Petit-Lancy, 1996), Vol. I, p. 420.

[6] R.S. Granetz, I.H. Hutchinson, J. Sorci, J. Irby, B. LaBombard, and D. Gwinn, Nucl. Fusion **36**, 545 (1996).

[7] J. Wesley, N. Fujisawa, S. Ortolani, S. Putvinski, M.N. Rosenbluth, and the ITER Joint Central Team, "Disruption, Vertical Displacement Event and Halo Current Characterization for ITER" in *16th International Conference on Fusion Energy, Montreal, 1996* (IAEA, Vienna, 1997), Vol. 2, p. 971.

[8] P. Noll, P. Andrew, M. Buzio, R. Litunovsky, T. Raimondi, V. Riccardo, and M. Verrecchia, "Present Understanding of Electromagnetic Behaviour during Disruptions in JET" in *19th Symposium on Fusion Technology, Lisbon* (JET Joint Undertaking, Abingdon, Oxon, UK, 1996), p. 73.

[9] J.H. Batteh, and G.E. Rolader, Phys. Fluids **31**, 1757 (1988).

[10] A.I. Morozov, and L.S. Solov'ev, "The Structure of Magnetic Fields", *Reviews of Plasma Physics*, edited by M.A. Leontovich (Consultants Bureau, New York, 1996), Vol. 2, p. 32.

[11] P.L. Taylor *et al.* in " DIII-D Disruption Studies", *Disruption and Vertical Displacement Event Characterization Workshop*, ITER Joint Work Site, Garching, Germany, February 1995.

[12] T.E. Evans, A.G. Kellman, D.A. Humphreys, M.J. Schaffer, P.L. Taylor, D.G. Whyte, T.C. Jernigan, A.W. Hyatt, and R.L. Lee, J. Nucl. Mater. **241-243**, 606 (1997).

Appendix A: Inductive coupling

The expression of inductive linkage given in Section B is only valid for a test loop placed near a current loop, a requirement quantified by restricting $k \approx 1$, where

$$k^2 = \frac{4a_z a_{z'}}{(a_z + a_{z'})^2 + (x + \delta_w)^2} \,, \tag{A1}$$

so that $0 \leq k \leq 1$ is always true. When the test loop is far from the current loop, or $k \to 0$, the flux linked is approximated by eqn. (3), where now

$$F_{zz'} = \frac{\pi}{2} \frac{(a_z a_{z'})^{3/2}}{[(a_z + a_{z'})^2 + (x + \delta_w)^2]^{3/2}} \,, \tag{A2}$$

which reduces to the inverse-cube dependence of a dipole field as $x \to \infty$.

The mutual inductances of the compound filaments of the halo change as the current paths expand along part of their perimeter inside a generally noncircular vessel. This is misrepresented by the above expressions, where circular rings expand along their entire perimeter, even if the initial self-inductance and its linear rate of change were correctly represented by a and l. It may be possible to devise different analytic approximations and include geometric factors. In realistic geometries however, the Biot-Savart law must be used directly within an appropriate numerical simulation.

Appendix B: Analytic approximation of the coupling integrals

We calculate approximate analytic expressions for the coupling integrals $I_1 - I_4$ on the basis of the short-range coupling coefficient only, given by eqn. (4). The magnitude of short-range coupling is much greater than that of long-range coupling, given by (A2). However, this approximation becomes progressively worse for large aspect ratios as the integrals are evaluated over an increasing number of far coils. The short-range coefficient drops rapidly, becoming zero at an inter-filament distance $d_r \equiv \mathcal{A}\Delta\bar{z}_r = 1.3$, at which point the approximation has clearly failed. The long-range coefficient decays more slowly. In the numerical simulation we included both near and far expressions, although we switched between them by simply taking the greater of the two. We further restrict the range of our analytic approximations by not considering very tight aspect ratios, that is, we adopt $\mathcal{A} > \mathcal{A}_t = 2d_r = 2.6$. Our evaluation of the coupling integrals is thus solely based on the short-range expression, over the toroidal range $[0,\ d_r]$.

It can be verified that the near coil coefficient can be approximated by

$$F_{zz'} \sim \ln d_r - \ln d \tag{B1}$$

while $F \sim |\ln d_0|$, where $d_0 = \delta/a \ll 1$, with δ the filament thickness. Using these expressions, and restricting $n < \mathcal{A}/2\pi d_0$, it is not difficult to show that integrals I_1, I_3 are given approximately by the expressions in (14, 16).

To evaluate I_2, I_4 we need an approximate expression for $M' = (\partial F/\partial\alpha)/F$. It may be verified, numerically or otherwise, that across $[0,\ d_r]$ we may take

$$F'_{zz'} \sim 1 \,, \tag{B2}$$

which is sufficient for our illustration purposes. The expressions in (15, 17) follow.

Appendix C: Calculation of the quality factor

We consider an annular wall sector between R_{in}, R_{out}, as in figure 7b, and assume $\partial_t = 0$, so that the current is curl-free. The current streamfunction then obeys

$$\nabla^2 f = 0\,, \qquad \text{where} \qquad i_R = \frac{1}{R}\frac{\partial f}{\partial \phi}\,, \qquad \text{and} \qquad i_\phi = -\frac{\partial f}{\partial R}\,. \tag{C1}$$

The solution of eqn. (C1) is of the form

$$f = \sum_n (A_n R^n + B_n R^{-n}) \sin(n[\phi - \zeta_n])\,, \tag{C2}$$

which may be evaluated given the current entering at the wall boundaries.

Considering a pure mode n, we may calculate the 'helical' fraction of the current by finding the value of f_n at an X-point, where $i_\phi = i_R = 0$. It is straightforward to show that X-points are located at

$$R_x = \sqrt{R_{in} R_{out}}\,, \qquad \text{and} \qquad \phi_x = \frac{\zeta}{2} + \frac{\pi}{n}(m + \frac{1}{2})\,, \tag{C3}$$

for $m = 0, 1, \ldots, 2n-1$. ζ, given by eqn. (25), is determined by the equilibrium magnetic field and is independent of n. By evaluating f_n at an X-point we may calculate the required ratio of the 'helical' amplitude to the total amplitude, as finally given by relation (26). The calculation automatically becomes three-dimensional if $\partial_t \neq 0$, because knowledge of the global quantity $\partial_t B$ normal to the wall is then required.

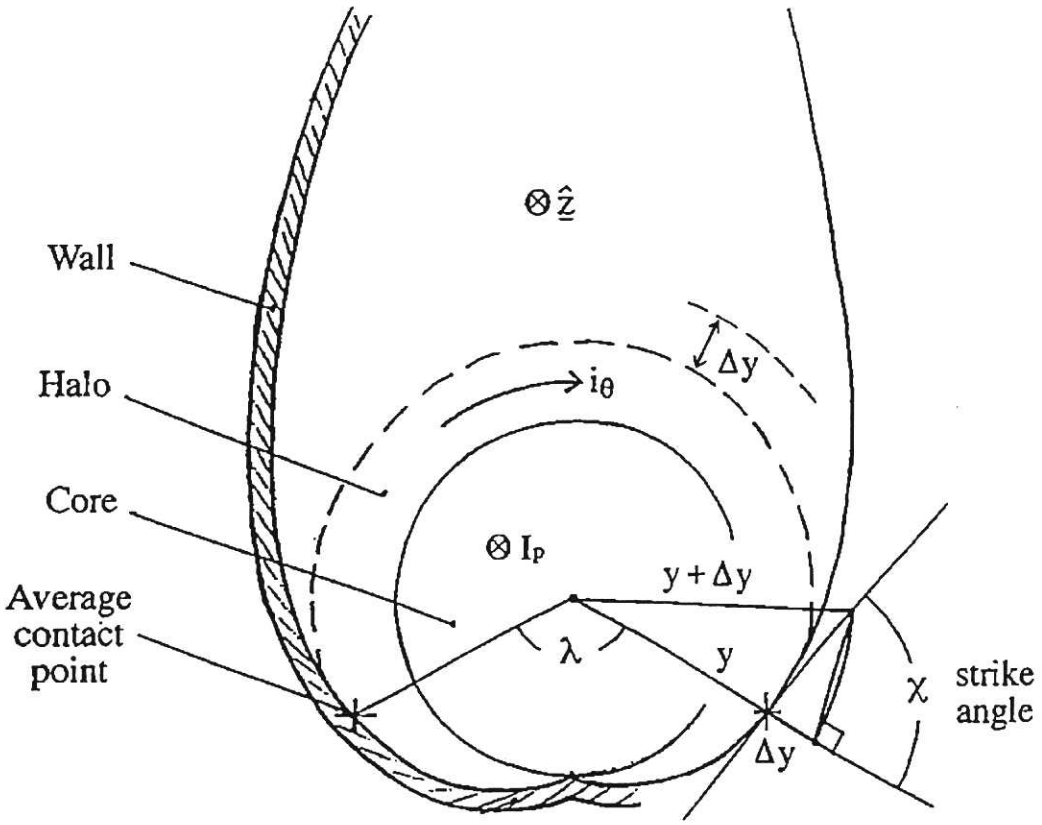

Figure 1a. Schematic poloidal cross-section of the plasma-wall circuit.

Shown are the basic elements and notation of the model.

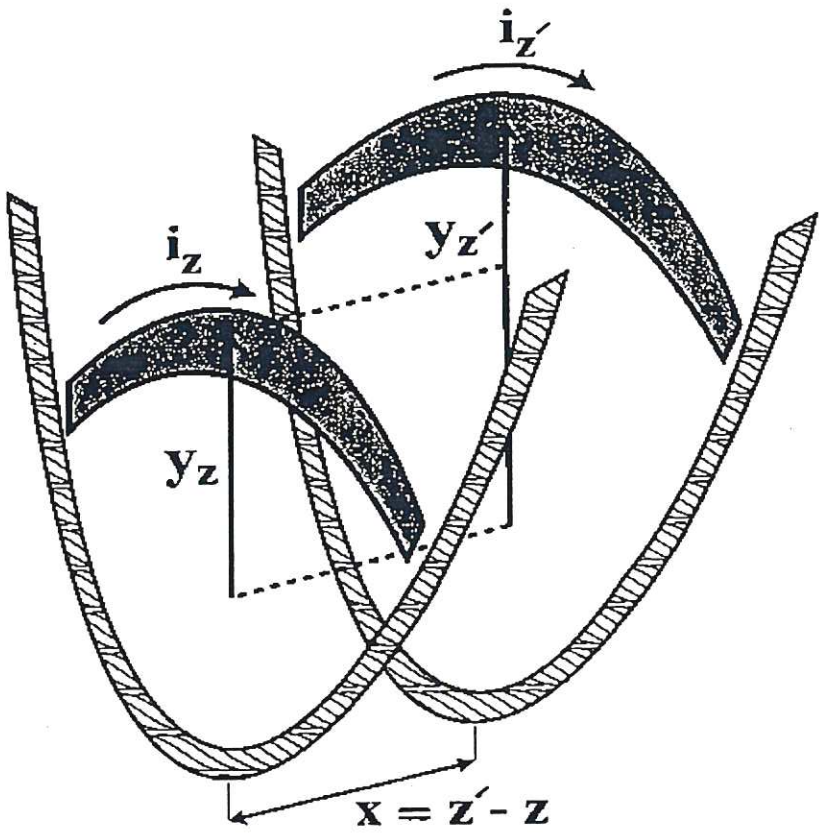

Figure 1b. Schematic of the toroidal arrangement of filaments.

The plasma paths at different toroidal positions make contact with the wall at different heights. The contacts slide up and down in response to force balance in the plasma, while the poloidal filaments are inductively linked.

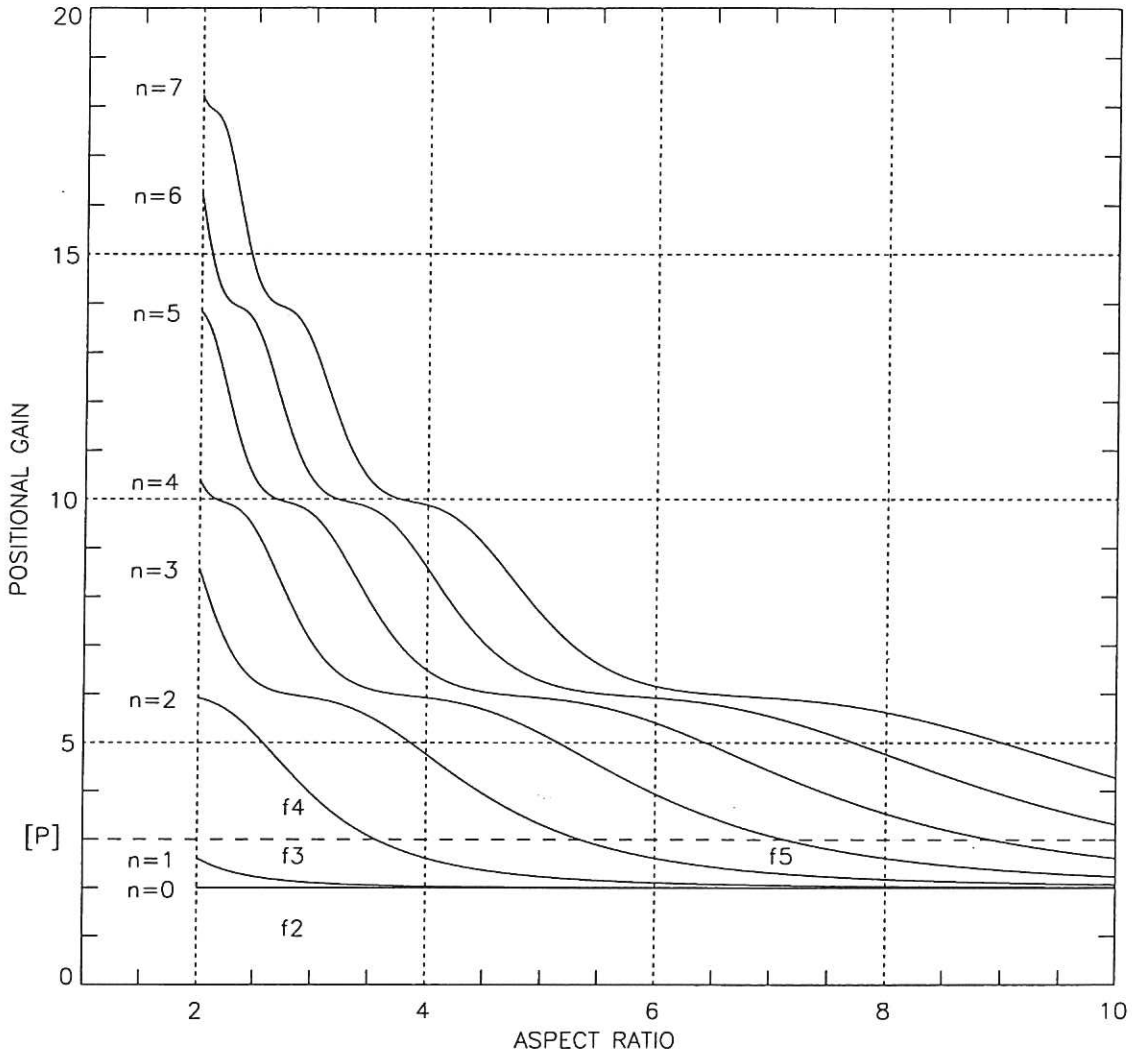

Figure 2. Analytic stability boundaries of the poloidal model.

Shown are the resonances of the first 8 harmonics of the instability on a diagram of positional gain s_0 versus inductive aspect ratio $\mathcal{A}$. At a resonance, when $R(\mathcal{A}, n) = 0$, see main text, the linear growth rate of a mode becomes singular. Our analytic approximations cannot take us to very low $\mathcal{A}$. The parameter P represents the ratio of the overall timescale of the halo circuit to an equivalent timescale of the local wall. For illustration we have chosen $P = 3$, indicated on the diagram by a dashed line. $s_0 = P$ is a universal cut-off, while a mode is unstable if s_0 lies between P and the corresponding resonance. Marked f2 to f5 on the graph are the positions corresponding to the numerical simulations presented in figures 3–6. The parameters of these simulations have been chosen not to contradict the details of this diagram, and are presented only to validate its general features.

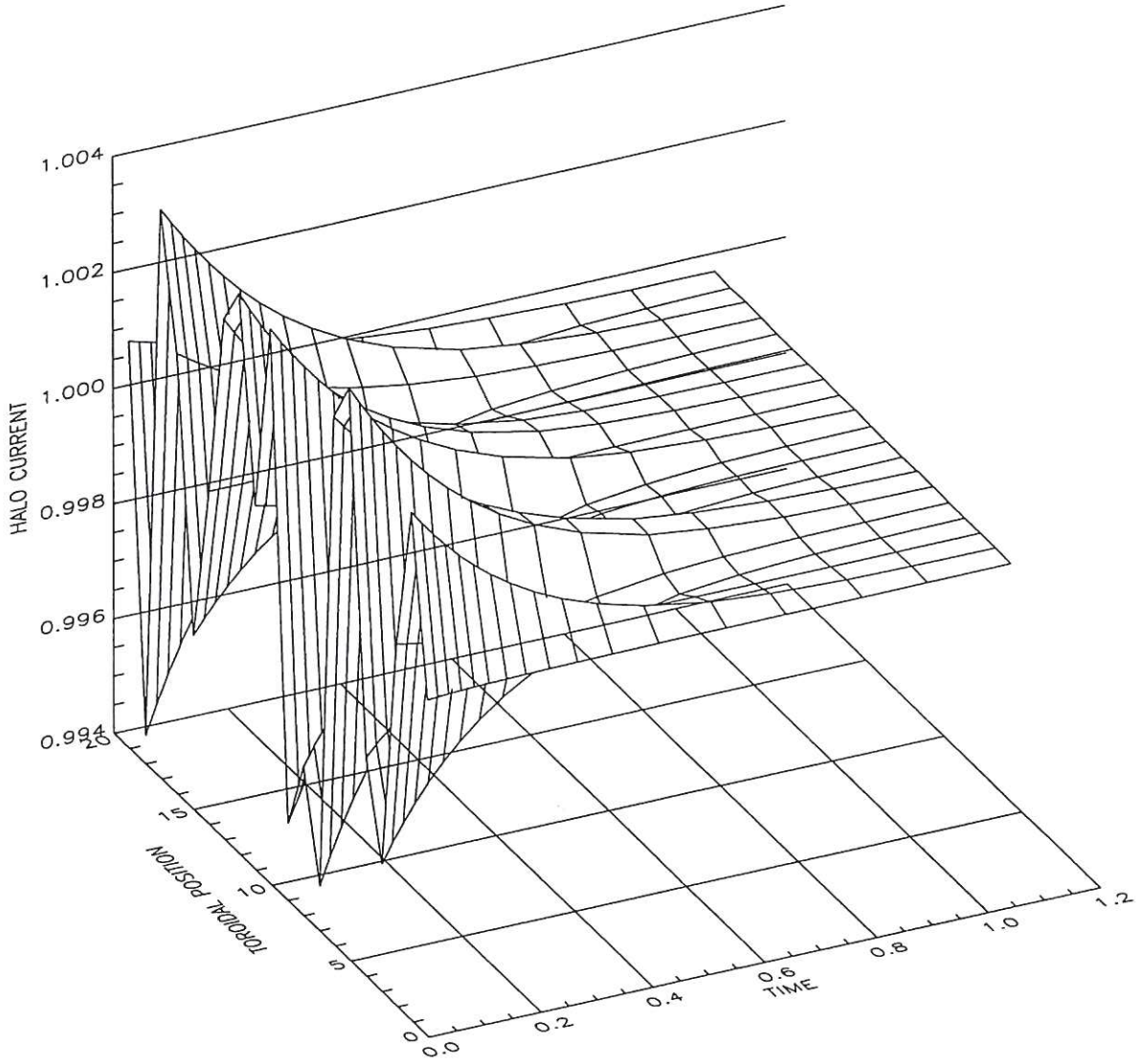

Figure 3. Case with universal stability.

Corresponding to f2 in figure 2, the positional gain in this case lies outside the interval $[P, R(\mathcal{A}, n)]$ for all n. As expected, an initial random perturbation decays to 1.0, the equilibrium value of current. Time in all figures is in units of τ_0, defined in the main text.

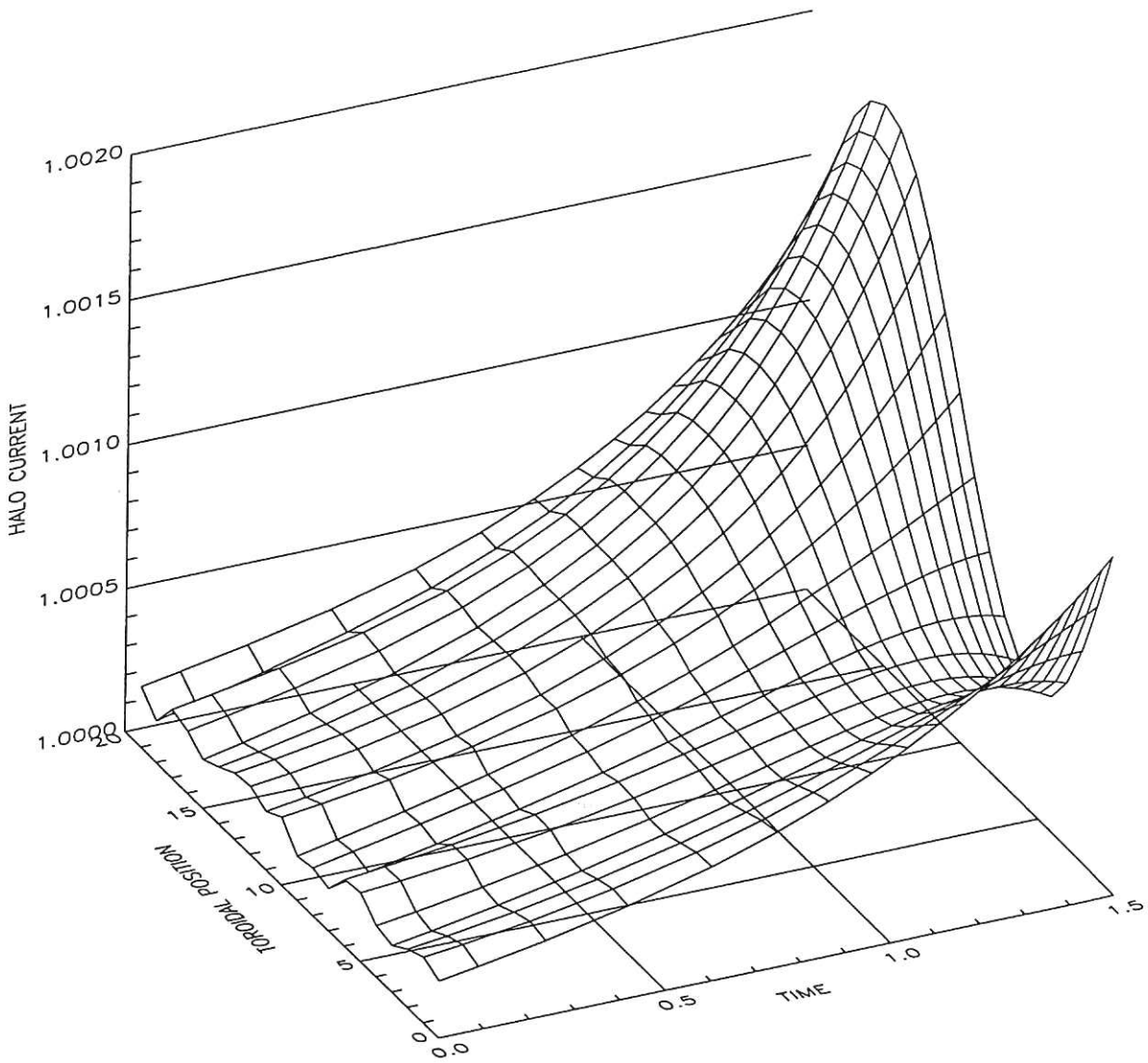

Figure 4. Instability with $n = 0$ and $n = 1$ dominant.

Corresponding to f3 in figure 2, a superposition of $n = 0$ and $n = 1$ grow out of a random initial perturbation, in accordance with the analytic expectation—see caption of figure 2 or main text. We have adjusted the initial values so that both components are visible. The resonances of the $n = 0$ and $n = 1$ are especially close, and tend to occur simultaneously.

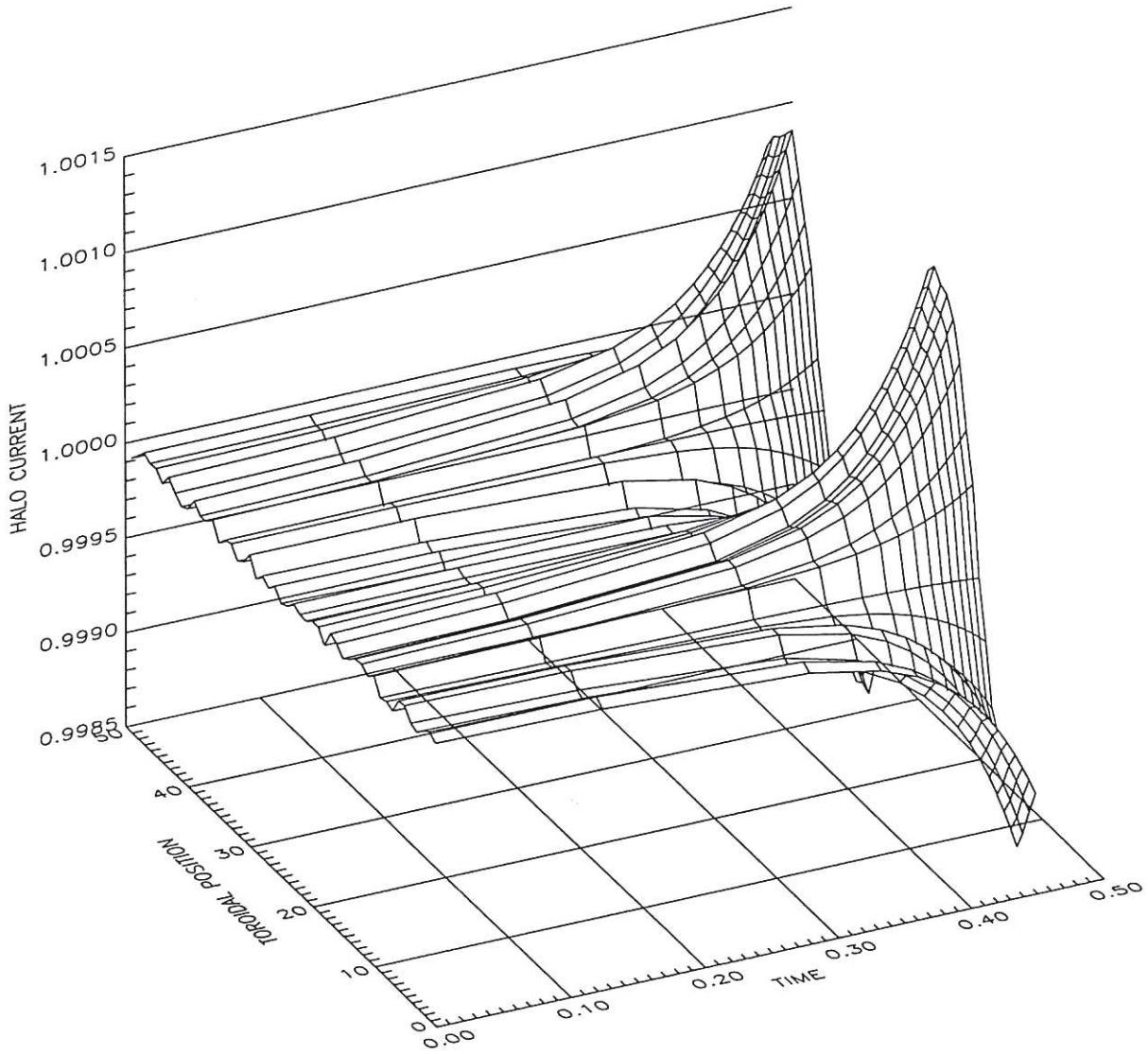

Figure 5. Instability with $n = 2$ dominant.

Corresponds to f4 in figure 2. A higher positional gain increases the mode number, at the same aspect ratio. If close to a resonance, the amplification of a single harmonic out of a random perturbation is expected to be extreme, as verified by the simulations. Away from a resonance, more harmonics are present.

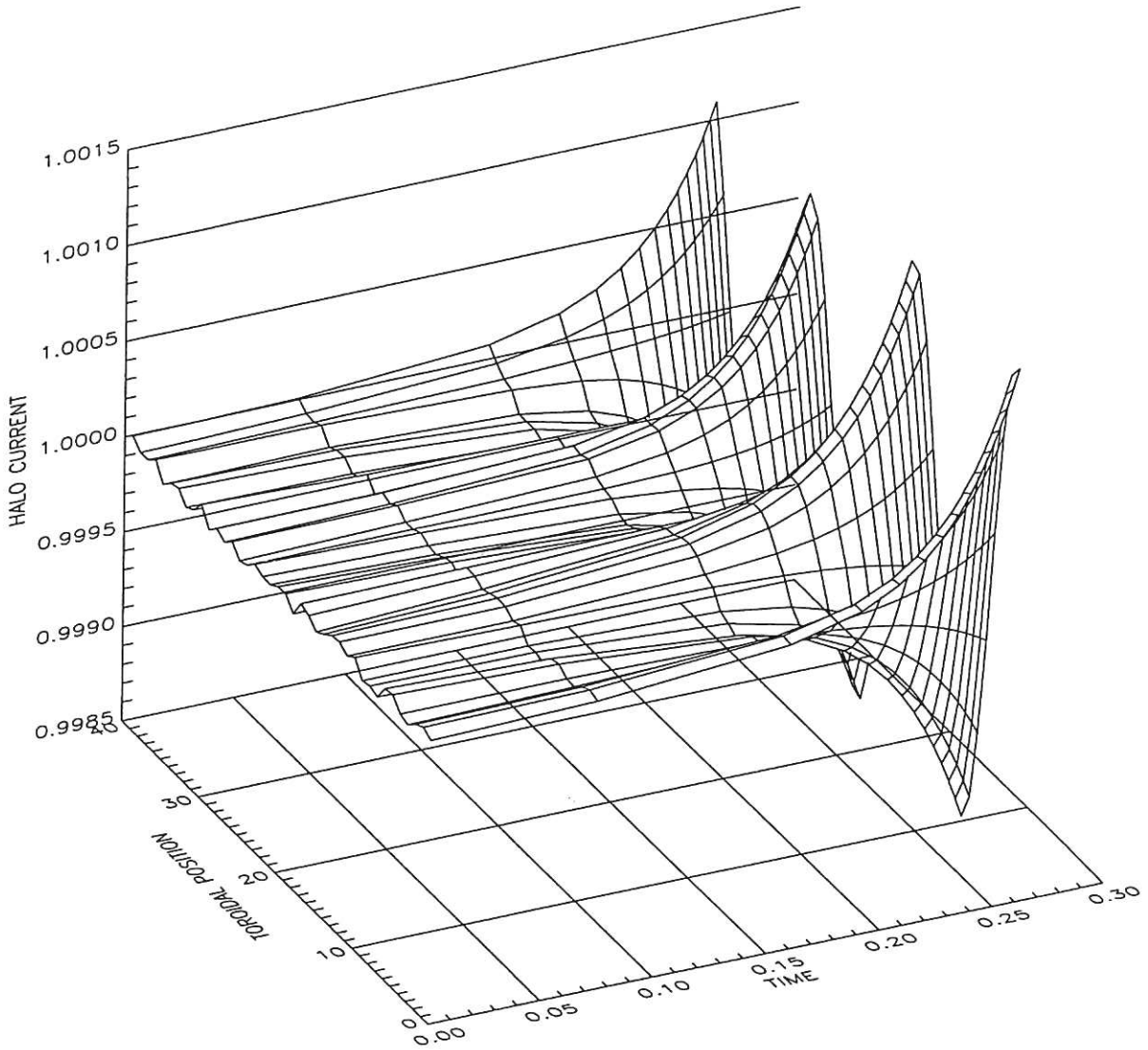

Figure 6. Instability with $n = 3$ dominant, at large aspect ratio.

Corresponds to f5 in figure 2. The positional gain is the same as for figure 4, but the aspect ratio has been increased from 2.75 to 7.0. As expected, the dominant mode changes from $n = 1$ to $n = 3$.

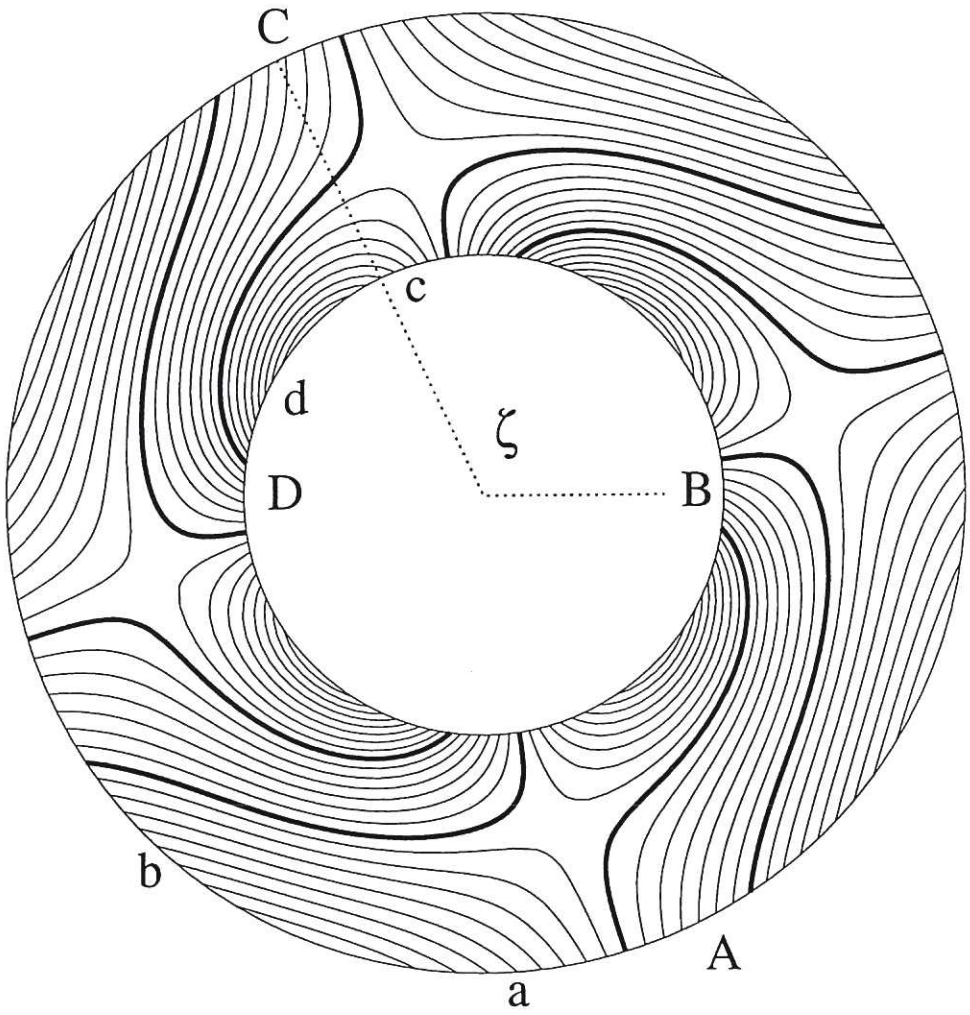

Figure 7a. Current flow in wall annulus.

Top view of toroidal wall sector with $n = 2$ stationary current streamfunction. The constant inboard-outboard phase difference ζ due to the plasma path (e.g. B to C, or b to c) is indicated by the dashed lines; thick lines highlight the 'helical' component of the flow. (ABCDA) and (abcda) mark helical and surface paths respectively.

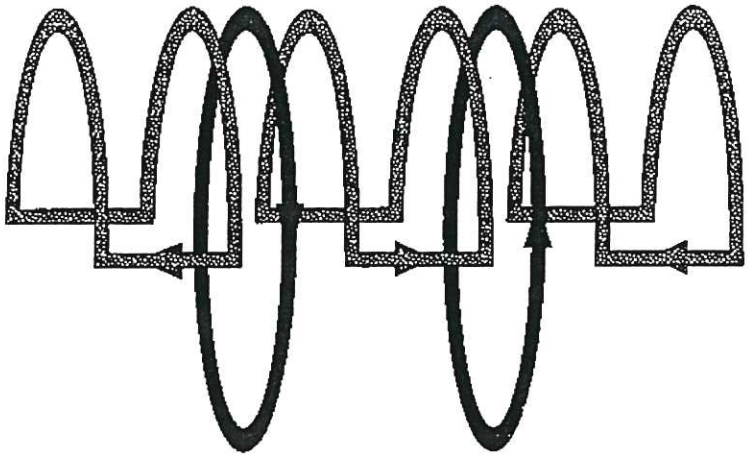

Figure 7b. Cartoon of the inductive topology of halo channels.
The diagram shows in a schematic way the splitting of mode current crossing the plasma-wall boundary into 'helical' and 'surface' channels (the upper part of the drawing corresponds to the plasma, and the lower to the wall). In reality, the helical loops link the plasma core both poloidally and toroidally, while the surface loops do neither. It can be verified, via figure 7a, that the distinction also holds for a helical halo.